This is a repository copy of *Self-Supplied Nano-Fusing and Transferring Metal Nanostructures via Surface Oxide Reduction*.

Article:

Self-Supplied Nano-Fusing and Transferring Metal Nanostructures via Surface Oxide Reduction

Jaeho Ahn[1,†], Ji-Won Seo[1,†], Jong Yun Kim[2], Jaemin Lee[1], Changsoon Cho[1], Juhoon Kang[1], Sung-Yool Choi[2], and Jung-Yong Lee[1,*]

[1]Graduate School of Energy, Environment, Water, and Sustainability (EEWS), Graphene Research Center, Korea Advanced Institute of Science and Technology (KAIST), Daejeon 305-701, Republic of Korea, [2]Department of Electrical Engineering, Graphene Research Center, Korea Advanced Institute of Science and Technology (KAIST), Daejeon 305-701, Republic of Korea

[†]These two authors contributed equally to this work.

[*]All correspondence should be addressed to J.-Y.L. (email: jungyong.lee@kaist.ac.kr)

Abstract

Here, we demonstrate that chemical reduction of oxide layers on metal nanostructures fuses junctions at nanoscale to improve the opto-electrical performance, and to ensure environmental stability of the interconnected nano-network. In addition, the reducing reaction lowers the adhesion force between metal nanostructures and substrates, facilitating the detachment of them from substrates. Detached metal nano-networks can be easily floated on water and transferred onto various substrates including hydrophobic, floppy, and curved surfaces. Utilizing the detached metal nanostructures, semi-transparent organic photovoltaics is fabricated, presenting the applicability of proposed reduction treatment in the device applications.

Introduction

Recently, transparent electrodes utilizing metallic nanomaterials such as silver nanowires (AgNWs), copper nanowires (CuNWs), and silver nanoparticles (AgNPs) have been reported as excellent alternatives to indium tin oxide (ITO), because of their high optoelectrical performance and mechanical robustness under bending and stretching conditions.[1–5] Various applications based on nanostructured electrodes have been reported, e.g., in light emitting diodes[6–8], photovoltaics[9–11], touch sensors[12–15], and actuators[16].

It is now well understood that the junctions of pristine metallic nanostructures are electrically unstable due to organic or oxide layers covering the nanomaterials, requiring further treatment for solid interconnection of the junction to attain higher conductivity. Post-treatments such as thermal annealing and mechanical pressing are conventionally applied for fusing the junction of nanomaterials.[1,17–19] Although these techniques connect the junctions and lower the sheet resistance R_{sh} of the electrode efficiently, fragile, flexible, or stretchable substrates cannot endure the accompanying high temperature or strain. Thus, mild post-treatments have been proposed including laser nano-welding[14], plasmonic welding[20], chemical welding[21], nanoparticle insertion[22], and hybridization[23–26].

However, these treatments cannot remove natural oxide layers existing on the surface of nanomaterials, which may impact on junction connection and the subsequent environmental stability of the metallic nanostructures. Moreover, if the metal nanostructure-based electrodes are exposed to air, continuous oxidation quickly increases the sheet resistance of the electrode.[27,28] Because the environmental vulnerability of the electrodes will adversely affect the reliability of the devices based on them, preventing the oxidation of the electrode is essential. Passivating the electrode by coating it with a chemically stable material blocks water and oxygen effectively, improving the air stability.[27,28] Yet, the passivation layer could lead to optical loss that causes performance degradation of optoelectronic devices.

Meanwhile, for flexible or stretchable electronics applications, the metallic nanostructure networks should be provided on substrates with hydrophobic, wrinkled, or curved surfaces; formation of them directly on the substrates is quite challenging.[2,13] Alternatively, transfer of the high quality electrodes using a supporting layer[29] or membrane filter can be used.[30] However, the sacrificial layers should be etched away to detach the nanostructures from the substrates or additional post-treatments to fuse the junctions is required.

We propose successive chemical reduction of natural oxide layers of metallic nanostructures as a novel post-treatment to interlock the junctions of the nano-network and even to assist the transfer process. With the successive reduction reaction, junctions are interconnected by ionized and diffused ions around the junction. Because the junctions are fused by self-supplied ions diffused from adjacent junction, additional ions or materials injection are not required. Accordingly, a high-performance AgNW electrode ($T = 93\ \%$, $R_{sh} = 17\ \Omega/\square$) was fabricated without any further treatment. Intriguingly, the fully interlocked junctions dramatically improved the AgNW chemical stability without optical loss. The increment in sheet resistance after exposure for 35 days in air was 10-fold lower than that of a non-treated AgNW reference electrode. The proposed versatile treatment can be equally applied to CuNWs and AgNPs for the same purpose. Furthermore, by immersing the reduced AgNWs into water, we were able to detach the AgNW network from the substrate and transfer it onto various types of substrates including curved glass, glove, leaf, and hydrophobic surfaces, thereby broadening the utility of AgNW electrodes to portable and wearable electronics. This transfer method was applied to the fabrication of semi-transparent organic photovoltaics (SOPVs) to illustrate its applicability.

Result and Discussion

Upon reacting with a reducing agent, the metal oxide on the surface of nanomaterials is ionized and leaves the nanomaterials negatively charged. A few angstroms oxide layer is reportedly formed on metallic nanomaterials surface upon exposure to air.[31] Because the junctions of nanomaterials have larger surface areas than other regions, electrons are concentrated at these junctions and induce a lower electrostatic potential.[21] (Figure S1) Therefore, ionized metal oxide originating from the surface of nanomaterials tends to diffuse to the junctions where it is recrystallized by the successive reduction, thereby interlocking the contact and reducing the sheet resistance. The proposed mechanism will be further proved below.

The proposed redox-reaction mechanism of the AgNWs is illustrated in Figure 1a. Upon reacting with vaporized hydrazine, the silver oxide covering the surface of AgNWs as an example of metal nanostructure (presented by red surfaces in Figure 1a(i)) is reduced to silver, and nitrogen and water are produced.[32]

$$2Ag_2O+N_2H_4 \rightarrow 4Ag + N_2 + 2H_2O \tag{1}$$

In order to investigate if there exists the oxide layer on the surface of nanomaterials, an energy-dispersive X-ray spectroscopy (EDS) mapping was conducted. (Figure 1b-i) The EDS mapping images for oxygen content confirm even fresh nanomaterials, AgNWs and CuNWs, have the surface oxidized.

Several reduction agents have been reacted including hydroquinone, sodium sulfite, sodium citrate, and hydrazine, all of which fused the junction and decreased the sheet resistance of the electrode. Hydrazine, which is widely used in various fields due to its effective reducing property[33,34], showed the highest decrease. (Figure S2) The extent to which the sheet resistance decreased for each reducing agent may be ascribed to their own reactivity. The standard reduction potential of hydrazine is higher than that of hydroquinone, sodium

citrate, and sodium sulfite meaning hydrazine has stronger reactivity, which can explain the highest decrease of sheet resistance by hydrazine.

Scanning electron microscopy (SEM) images illustrate the effect of the chemical reduction on the AgNWs, as shown in Figure 2a and b. The junctions were well fused after the reduction treatment compared to the as-prepared AgNWs. (Figure 2b) Transmission electron microscopy (TEM) images in the insets also reveal the coalescing effect. In as-sprayed AgNWs, two adjacent silver nanowires simply overlapped and the boundaries of the upper and lower AgNW are clearly distinguished. Figure 2c illustrates the junction of non-treated and chemically reduced AgNWs. Cross-sectional SEM image in Figure 2d shows as-sprayed AgNWs are separated (indicated by a white arrow). In contrast, the junction of reduced AgNWs is completely fused without boundary between the AgNWs. (Figure 2e) Inset images schematically illustrate the cross-sectional junction of AgNWs and Figure S3 shows the cross-sectional SEM images for each position. Figure S4 shows TEM images and fast furrier transform (FFT) analysis of the junction of as-deposited and reduced AgNWs. In contrast to as-deposited AgNW network that are not fused, poly-crystal silver precipitation is shown at the junction of reduced AgNWs. FFT analysis of non-reduced AgNWs (Figure S4f) at junction shows crystallinity of upper and lower AgNWs, while that of reduced AgNWs (Figure S4g) does not, suggesting the poly-crystallinity. The silver ions originate from the surface *near* the junction, not only *at* the junction. The ionized Ag is concentrated near the junction because the junction has lower electrostatic potential than other region. It should be noted that it took less than an hour to spray fresh AgNWs on substrates and perform the chemical reduction treatment, suggesting that newly prepared AgNWs have enough Ag_2O to react with reducing agents for interlocking the junction. Simple experiment was conducted for proving the recrystallizing by the reducing agent. The silver nitrate dissolved methyl alcohol was prepared and hydrazine solution was dropped into the methyl alcohol. Right then,

5

crystalized Ag was observed in the solution, supporting the ionized Ag ions are reduced and recrystallized by the reduction agent. (Figure S5)

To further investigate the effect of the reducing agents on AgNWs, the AgNW network was intentionally oxidized by O_2 plasma at 90 W for 10 min and reduced again by hydrazine. SEM images taken at the same position after each treatment showed the AgNW thickness variation attributed to the varying thickness of the oxide layer. (Figure 3a) Average diameter d_{avg} values and blue colored AgNWs present the varied thickness after each treatment. The oxygen content (in wt.%) measured by EDS becomes higher after the plasma treatment and is lowered again by the hydrazine treatment. (Figure 3b) Concerning the electrical conductivity, the sheet resistance became immeasurable as soon as the AgNWs (initial R_{sh}: 1 Ω/□) were oxidized by the O_2 plasma. Subsequently, when the oxidized AgNWs were reduced by hydrazine, the initial sheet resistance value of 1 Ω/□ was recovered. The oxide content and sheet resistance variations reveal that hydrazine reduces silver oxide and the junction blocked by the oxide layer can be interlocked by reduction. It should be noted that other selective fusing treatments using plasmonic local heating, nanoparticle growth or etching Ag with Cl ion cannot remove the oxidized layer; these approaches would work only on newly prepared AgNWs.[20–22]

Utilizing the reducing property, the AgNW electrode optoelectrical characteristics were enhanced as shown in Figure 3c. Samples with the same initial sheet resistance and transmittance (7 Ω/□, 84 %) were prepared and treated for different periods of time. Initially, the sheet resistance decreased due to the onset of interlocking of the AgNWs during the reduction process; however, this trend was reversed after 7 min. The increasing sheet resistance is attributed to AgNWs disconnections emerging in the elongated reduction process. As illustrated in the inset SEM images in Figure 3c, the persistent migration of atoms in water, by-product of the reduction process (Eq. 1), at the surface of AgNWs makes the wire agglomerated during elongated reaction because the overall AgNW volume is fixed.

Moreover, surface tension of water on the AgNWs tends to form droplets, resulting in disconnections of AgNWs. Contrary to the sheet resistance, the transmittance is hardly changed by the chemical reduction. The slight increment in transmittance can be ascribed to the thinning effect of the AgNWs by surface diffusion.

By applying the optimal reduction period, the AgNW electrodes with enhanced optoelectrical characteristics were fabricated. Figure 3d illustrates that the successive reduction treatment is compared with previously reported techniques; it shows excellent optoelectrical performance. ($T = 93$ % and $R_{sh} = 17$ $\Omega/\square$) Outstanding optoelectrical performance is attributed to the removal of the oxide layer between the nanowires to fuse junctions completely. Comparison with previously proposed approaches is summarized in Table S1.

To prove the benefit of our approach, the optoelectrical characteristics of as-sprayed, thermally annealed (230 °C, 20 min), graphene oxide (GO)-coated, and hydrazine-treated AgNWs are compared in Figure S6a. It should be noted that our AgNWs junctions are partially fused even before post-treatment because of washing, filtering and spraying processes, which yield high opto-electrical performance.[35] Therefore, the change of the sheet resistance by post-treatment can be relatively small. Nonetheless, the hydrazine-treated electrode outperforms the as-sprayed, GO-coated, and even the thermally-annealed electrodes. Figure S6b and S7 show the hydrazine treatment brought about the highest and consistent decrement in sheet resistance for AgNW networks of different density. Although GO decreases the sheet resistance of AgNWs by wrapping the junctions, it does not seem to cover all AgNW junctions if their density is too high. Moreover, thicker GO would decrease the transmittance, thereby deteriorating the optoelectrical performance. Thermal annealing is also affected by the density of AgNWs because the heat transfer from the substrate to individual AgNWs can vary with the AgNW layer thickness. Hydrazine treatment in vapor phase, however, is not affected by the AgNW density or geometry, and the transmittance is not

affected by the reducing reaction, thus maintaining the high optoelectrical performance. As shown in Figure S8, subsequent hydrazine treatment after thermal annealing decreased R_{sh} of the electrode further, which proves the advantage of vaporized treatment as well as the merit of removing the oxide layers that hinder the junction connection. The ratio of the DC to the optical conductivity σ_{DC}/σ_{Op} as a figure of merit of as-sprayed, thermally annealed, GO-coated, and hydrazine-treated AgNWs is 321, 374, 340, and 435, respectively.[36] We also compared our approach with one of junction fusing processes (NaCl treatment for 40 s); hydrazine treated AgNWs for 40 s showed higher R_{sh} decrement as shown in Figure S9.[21]

Interestingly, the AgNW-electrode reduction treatment improved environmental stability. Oxidation of AgNW electrodes without proper overcoatings increases their sheet resistance.[27,37] Specifically, the oxidized layers at the AgNWs junctions cause higher junction and sheet resistance, because the junction resistance affects the sheet resistance more sensitively than the bulk resistance. Figure 2c schematically illustrates that if the junction gap is filled with migrated Ag, the junction resistance will not be affected by subsequent oxidation. However, the junction resistance of the non-treated AgNWs would further increase because of oxidation. Figure 4a shows that the reduced electrode presents 10-fold lower increment in sheet resistance than the non-treated AgNWs, being even 6-fold lower than that of the GO-coated electrodes after 35 days. Although GO prohibits the contact with water and oxygen effectively, galvanic corrosion can degrade the metal, bringing oxidation of the electrode.[38] The small increase in the sheet resistance of the reduced sample in air is attributed to surface oxidation of the nanowires. It should be noted that thermal annealing of AgNWs bringing about interconnection to the junctions as well as surface oxidation showed better stability than as-sprayed AgNWs, revealing that junction interlocking is more important for the environmental stability than surface oxidation. (Figure S10) The sheet resistance of the as-sprayed AgNWs after 100 days was immeasurably high due to oxidation. After reducing, interestingly, the sheet resistance recovered to the same value as that of the hydrazine-treated

sample (dashed line in Figure 4a), implying that the oxidized layer blocking the conduction across the junction was removed. With our proposed reduction process, therefore, AgNW electrode deposited on substrates can be stored in ambient conditions because oxidized AgNWs can be recovered at any time.

To confirm the role of the junction interconnections on the AgNWs stability, the junctions were intentionally disjointed by stretching the AgNWs.[8] Figure 4b presents the sheet resistance of the stretched AgNWs is increased faster than that of non-stretched AgNWs for both non-treated and hydrazine-treated electrodes. Because the junctions are disrupted by tensile strain, oxidation starts at the junctions and thereby the increase in the sheet resistance is accelerated. The result of the stretched AgNWs proves the importance of the junction´s interconnections on the stability and therefore, consistent mechanical strain on AgNWs can deteriorate the environmental stability of the electrode.

The proposed reduction treatment was applied to such nanomaterials as CuNWs and assembled AgNPs. EDS mapping images also confirm existence of the oxide layer on the surface of as-prepared CuNWs. (Figure 1h) Figure 5a and b reveal the junction of CuNWs before and after reduction treatment. Upon applying the proposed treatment, the junction of CuNWs transparent electrode was also fused, achieving the high optoelectrical performance ($T = 85.5$ %, $R_{sh} = 53$ $\Omega/\square$) without any other post-treatments; this is comparable to that of CuNWs treated with other post-treatments. (Figure S11) Opto-electrical performance change with respect to the reduction time is similar to the AgNWs case. (Figure 5c) The faster reaction may be ascribed to relatively higher reactivity of CuNWs than that of AgNWs. Figure 5d exhibits excellent environmental stability of the hydrazine treated CuNWs compared to that of non-treated CuNWs. Moreover, the proposed reduction process also fused AgNPs. Immeasurable sheet resistance of closely packed neat AgNPs due to high contact resistance became 7 $\Omega/\square$ after fusing with reduction. Figure S12 shows the SEM images of

9

assembled AgNPs before and after reduction. These results suggest that the proposed reduction technique can be applied to various metallic nanomaterials and nanostructures.

Besides the junction interlocking, water is generated as a reaction byproduct on the AgNW surface and lowers the adhesive force between them and the substrate. If the AgNWs on a substrate are immersed into water after reduction but before being dried, the bare AgNW network can float on the water. Figure 6a shows the floating AgNWs and the substrate sunken into the bath. Because the AgNWs are fused and tightly bound, they are not dispersed and do not sink. Figure 6b–e show that the floating AgNW electrode can be transferred on various substrates, such as hydrophobic or wrinkled surfaces, polymers having low melting temperature, gloves, curved glass, and a leaf. Usually, the AgNW electrode is difficult to form directly on such substrates because of their surface properties. However, by using the transfer process, uniform AgNW networks can be formed on it. Moreover, because the AgNWs are already fused prior to the transfer, no additional post-treatment is needed. Transferring the AgNW network on glove shows the possibility of applying this electrode to wearable devices, for example directly on clothes. Even patterned letters using AgNWs were successfully transferred to the centrifuge tube. (Figure 6f and S13) The lighting LED connected with a battery *via* the AgNW electrodes implies that the AgNW network was not damaged during the transfer process onto the curved surface. (Figure 6g) Indeed, the sheet resistance does not change after the transfer process. Although the adhesion of as-transferred AgNWs to the substrate is weak similar to that of bar-coated, spray-coated or spin-coated AgNWs, it can be promoted with adhesive layers.

Utilizing the transfer process of AgNWs, AgNWs were transferred on organic layers to fabricate semi-transparent organic photovoltaics (SOPVs). The inset of Figure 7a illustrates the structure of the SOPVs using AgNWs as top electrode. The device structure is glass / ITO / ZnO / PTB7:PC$_{70}$BM / PEDOT:PSS / AgNW electrode. The AgNW electrode was transferred on top of the PEDOT:PSS layer and compared with a device using directly

sprayed AgNWs.[39–41] Figure 7a shows the J–V characteristics of the SOPVs. The SOPV with

transferred AgNWs shows higher power conversion efficiency (PCE) of 3.11 % than the

SOPV with sprayed AgNWs (2.12 %) due to its improved fill factor (FF), because the

transferred AgNW electrode had lower sheet resistance by the interlocking of the AgNW

junctions as a result of the hydrazine treatment compared to the sprayed AgNW electrode.[42,43]

The short circuit current (J_{sc}) of the SOPV with transferred AgNWs was lower than that of the

reference device due to the reduced absorption of the active layers as shown in Figure 7b. The

average transmittance at wavelengths in the range of 400–800 nm was approximately 47 %.

The lower FF of the AgNW device was probably caused by the incomplete electrical contact

between PEDOT:PSS and AgNW electrode.[44] The photovoltaic performance is summarized

in Table 1.

Conclusion

To conclude, a novel post-treatment method for fusing the metallic nanomaterials was proposed. By chemically reducing the oxide layer existing on the surface of metal nanostructures using vaporized reducing agents, the AgNW junctions were interconnected effectively and high-performance transparent electrodes were fabricated with enhanced the stability. The proposed post-treatment method is also applied to CuNWs and AgNPs to cause junction interlocking. Furthermore, the reduced AgNW networks were easily detached from the original substrate and transferred onto various other substrates, allowing the AgNWs to be used in the fabrication of SOPVs. The proposed post-treatment technique can facilitate the fabrication of wearable devices and broadens the applicability of metallic nanomaterials in various fields.

Experimental Procedures

Materials preparation: AgNWs were synthesized based on a modified polyol process and prepared on the substrates in the same way as reported in previous reports.[35,45] Diameter and length are 60-80 nm and 15-30 μm, respectively. CuNWs were synthesized based on the previous report.[46] Graphene oxide solution was prepared based on modified Hummer's method and silver nanoparticle is synthesized following a modified polyol method.[47,48]

Sample preparation: To fabricate the AgNW or CuNW electrodes, the AgNWs or CuNWs solution is sprayed on the substrates using a lab-built spray system, which can move along x and y directions, following preset trajectory. While the solution is sprayed, the substrate is placed on 100 °C hot plate in order to evaporate the solvent. By controlling the density of AgNW or CuNW solution and the number of trajectories, AgNW or CuNWs electrodes having various densities are fabricated. AgNP film is prepared by convective assembly method.[49]

Reduction of the metal nanowires electrode: 30 mM of each sodium sulfite, sodium citrate, and hydroquinone is prepared in deionized (DI) water. Hydrazine hydrate solution (45% in DI water) was purchased from Sigma Aldrich. The water bath was heated to 80 °C and the beaker containing 1 ml of reducing agent and the sample tray was put into the water bath.

Other post-treatment processes: To anneal the AgNWs thermally, the AgNW electrode is placed on a hot plate at 230 °C for 20 min. To prepare AgNWs / GO hybrid films, 0.05 wt% GO was spun at 500 rpm for 5 s, subsequently at 1500 rpm for 30 s, and finally dried on a hot plate at 120 °C for 10 min.

Durability test: AgNW electrodes treated by different methods were placed under an ambient condition on a laboratory table for over 100 days. Average temperature and humidity were 22 °C and 24 %, respectively.

Stretching the AgNW electrodes: To stretch the AgNW electrodes, AgNWs sprayed on polyimide (PI) films and AgNWs / PI films were 20 % stretched uniaxially and released using a lab-made stretching instrument.

Preparation of SOPVs: On pre-cleaned ITO glass, a zinc oxide (ZnO) layer was spun at 6000 rpm for 30 s that was then annealed at 200 °C for 1 h on a hot plate. Subsequently, a solution of PTB7:PC$_{70}$BM at the weight ratio of 1:1.5 in chlorobenzene with 3 vol% of 1,8-diiodooctane (DIO) was spun at 3500 rpm for 30 s on the ZnO layer.[47,50,51] Next, PEDOT:PSS (Al4083, Clevios) diluted in 2-propanol (Sigma Aldrich) at 1:5 weight ratio was spun on the active layer at 3000 rpm for 30 s. Then, the AgNWs floating on water (R$_{sh}$: 5 Ω/□) were scooped up on the PEDOT:PSS layer. Subsequently, a further PEDOT:PSS layer diluted in 2-propanol was spun once again. For comparison, an otherwise identical device using spray-deposited AgNWs was prepared by spraying the AgNWs in methanol directly onto the PEDOT:PSS layer on a hot plate (40 °C). The reference OPV was produced by placing the PEDOT:PSS-coated device into a vacuum chamber (< 3×10^{-7} Torr) and a thin Ag film (150 nm) was evaporated. The device area was 15 mm^2. The OPVs were illuminated at the

intensity of 100 mW/cm^2 using a solar simulator with AM 1.5G filter (PEC-L12, Peccell Technologies) and then the current density–voltage (*J–V*) characteristics were measured.

Characterization: SEM images were acquired using field-emission scanning electron microscopy (FE-SEM, Nova230, FEI Co.) and EDS data were also obtained using FE-SEM (Sirion, FEI Co.). Transmission electron microscopy (TEM) and EDS mapping were taken on the instrument FE-TEM (Tiatan cubed G2 60-300, FEI Co.). The sheet resistance was measured using a 4-point probe sheet resistance meter and the transmittance by a UV-vis spectrophotometer (UV-3600, Shimadzu) equipped with an integrating sphere. Transmittance data is averaged (400 ~ 800 nm) with reference to a glass substrate. Cross-sectional images of the AgNW junctions were prepared using focused ion beam (Helios NanoLab 450 F1, FEI Co.).

Supporting information

Simulation for electrostatic potential at the junction of AgNWs; Graph of sheet resistance change with respect to various reducion materials; Cross-sectional SEM images of AgNWs junction before and after reduction; TEM images of AgNWs after reduction; AgNO$_3$ dissolved solution before and after dropping hydrazine solution; Opto-electrical performance comparison with different post-treatment methods; Sheet resistance decrement distribution after reduction treatment; Comparison of change of sheet resistance after thermal annealing and additional hydrazine treatment; Comparison of decrement of sheet resistance of the hydrazine and NaCl chemical treatment; Photographs AgNW electrodes after 20 days; Comparison of optoelectrical performance of hydrazine treated CuNWs with other treatments; Top view of SEM images of AgNPs (a) before and (b) after reduction treatment; Photographs of a PET mask and patterned letters of AgNWs; Comparison of various post-treatments for fusing of metal nanostructures

Acknowledgements

References

(1) Lee, J.-Y.; Connor, S. T.; Cui, Y.; Peumans, P. Solution-Processed Metal Nanowire Mesh Transparent Electrodes. *Nano Lett.* **2008**, *8* (2), 689–692.

(2) Akter, T.; Kim, W. S. Reversibly Stretchable Transparent Conductive Coatings of Spray-Deposited Silver Nanowires. *ACS Appl. Mater. Interfaces* **2012**, *4* (4), 1855–1859.

(3) Xu, F.; Zhu, Y. Highly Conductive and Stretchable Silver Nanowire Conductors. *Adv. Mater.* **2012**, *24* (37), 5117–5122.

(4) Im, H.-G.; Jung, S.-H.; Jin, J.; Lee, D.; Lee, J.; Lee, D.; Lee, J.-Y.; Kim, I.-D.; Bae, B.-S. Flexible Transparent Conducting Hybrid Film Using a Surface-Embedded Copper Nanowire Network: A Highly Oxidation-Resistant Copper Nanowire Electrode for Flexible Optoelectronics. *ACS Nano* **2014**, *8* (10), 10973–10979.

(5) Park, K.-T.; Park, J.; Park, J.-W.; Hwang, J. Maskless, Site-Selective, Nanoaerosol Deposition via Electro-Aerodynamic Jet to Enhance the Performance of Flexible Ag-Grid Transparent Electrodes. *RSC Adv.* **2015**, *5* (56), 44847–44852.

(6) Gaynor, W.; Hofmann, S.; Christoforo, M. G.; Sachse, C.; Mehra, S.; Salleo, A.; McGehee, M. D.; Gather, M. C.; Lüssem, B.; Müller-Meskamp, L.; Peumans, P.; Leo, K. Color in the Corners: ITO-Free White OLEDs with Angular Color Stability. *Adv. Mater.* **2013**, *25* (29), 4006–4013.

(7) Yu, Z.; Zhang, Q.; Li, L.; Chen, Q.; Niu, X.; Liu, J.; Pei, Q. Highly Flexible Silver Nanowire Electrodes for Shape-Memory Polymer Light-Emitting Diodes. *Adv. Mater.* **2011**, *23* (5), 664–668.

(8) Liang, J.; Li, L.; Tong, K.; Ren, Z.; Hu, W.; Niu, X.; Chen, Y.; Pei, Q. Silver Nanowire Percolation Network Soldered with Graphene Oxide at Room Temperature and Its Application for Fully Stretchable Polymer Light-Emitting Diodes. *ACS Nano* **2014**, *8* (2), 1590–1600.

(9) Yu, Z.; Li, L.; Zhang, Q.; Hu, W.; Pei, Q. Silver Nanowire-Polymer Composite Electrodes for Efficient Polymer Solar Cells. *Adv. Mater.* **2011**, *23* (38), 4453–4457.

(10) Jin, J.; Lee, J.; Jeong, S.; Yang, S.; Ko, J.-H.; Im, H.-G.; Baek, S.-W.; Lee, J.-Y.; Bae, B.-S. High-Performance Hybrid Plastic Films: A Robust Electrode Platform for Thin-Film Optoelectronics. *Energy Environ. Sci.* **2013**, *6* (6), 1811–1817.

(11) Won, Y.; Kim, A.; Lee, D.; Yang, W.; Woo, K.; Jeong, S.; Moon, J. Annealing-Free Fabrication of Highly Oxidation-Resistive Copper Nanowire Composite Conductors for Photovoltaics. *NPG Asia Mater.* **2014**, *6* (6), e105.

(12) Lee, J.; Lee, P.; Lee, H. B.; Hong, S.; Lee, I.; Yeo, J.; Lee, S. S.; Kim, T.-S.; Lee, D.; Ko, S. H. Room-Temperature Nanosoldering of a Very Long Metal Nanowire Network by Conducting-Polymer-Assisted Joining for a Flexible Touch-Panel Application. *Adv. Funct. Mater.* **2013**, *23* (34), 4171–4176.

(13) Lee, H.; Lee, K.; Park, J. T.; Kim, W. C.; Lee, H. Well-Ordered and High Density Coordination-Type Bonding to Strengthen Contact of Silver Nanowires on Highly Stretchable Polydimethylsiloxane. *Adv. Funct. Mater.* **2014**, *24* (21), 3276–3283.

(14) Lee, J.; Lee, P.; Lee, H.; Lee, D.; Lee, S. S.; Ko, S. H. Very Long Ag Nanowire Synthesis and Its Application in a Highly Transparent, Conductive and Flexible Metal Electrode Touch Panel. *Nanoscale* **2012**, *4* (20), 6408–6414.

(15) Hong, S.; Yeo, J.; Kim, G.; Kim, D.; Lee, H.; Kwon, J.; Lee, H.; Lee, P.; Ko, S. H. Nonvacuum, Maskless Fabrication of a Flexible Metal Grid Transparent Conductor by Low-Temperature Selective Laser Sintering of Nanoparticle Ink. *ACS Nano* **2013**, *7* (6), 5024–5031.

(16) Yun, S.; Niu, X.; Yu, Z.; Hu, W.; Brochu, P.; Pei, Q. Compliant Silver Nanowire-Polymer Composite Electrodes for Bistable Large Strain Actuation. *Adv. Mater.* **2012**, *24* (10), 1321–1327.

(17) Tokuno, T.; Nogi, M.; Karakawa, M.; Jiu, J.; Nge, T. T.; Aso, Y.; Suganuma, K. Fabrication of Silver Nanowire Transparent Electrodes at Room Temperature. *Nano Res.* **2011**, *4* (12), 1215–1222.

(18) Chen, Z.; Ye, S.; Stewart, I. E.; Wiley, B. J. Copper Nanowire Networks with Transparent Oxide Shells That Prevent Oxidation without Reducing Transmittance. *ACS Nano* **2014**, *8* (9), 9673–9679.

(19) Park, J. H.; Lee, D. Y.; Seung, W.; Sun, Q.; Kim, S.-W.; Cho, J. H. Metallic Grid Electrode Fabricated via Flow Coating for High-Performance Flexible Piezoelectric Nanogenerators. *J. Phys. Chem. C* **2015**, *119* (14), 7802–7808.

(20) Garnett, E. C.; Cai, W.; Cha, J. J.; Mahmood, F.; Connor, S. T.; Greyson Christoforo, M.; Cui, Y.; McGehee, M. D.; Brongersma, M. L. Self-Limited Plasmonic Welding of Silver Nanowire Junctions. *Nat. Mater.* **2012**, *11* (3), 241–249.

(21)   Lee, S. J.; Kim, Y.-H.; Kim, J. K.; Baik, H.; Park, J. H.; Lee, J.; Nam, J.; Park, J. H.; Lee, T.-W.; Yi, G.-R.; Cho, J. H. A Roll-to-Roll Welding Process for Planarized Silver Nanowire Electrodes. *Nanoscale* **2014**, *6* (20), 11828–11834.

(22)   Lu, H.; Zhang, D.; Ren, X.; Liu, J.; Choy, W. C. H. Selective Growth and Integration of Silver Nanoparticles on Silver Nanowires at Room Conditions for Transparent Nano-Network Electrode. *ACS Nano* **2014**, *8* (10), 10980–10987.

(23)   Zhu, R.; Chung, C.-H.; Cha, K. C.; Yang, W.; Zheng, Y. B.; Zhou, H.; Song, T.-B.; Chen, C.-C.; Weiss, P. S.; Li, G.; Yang, Y. Fused Silver Nanowires with Metal Oxide Nanoparticles and Organic Polymers for Highly Transparent Conductors. *ACS Nano* **2011**, *5* (12), 9877–9882.

(24)   Kholmanov, I. N.; Domingues, S. H.; Chou, H.; Wang, X.; Tan, C.; Kim, J.-Y.; Li, H.; Piner, R.; Zarbin, A. J. G.; Ruoff, R. S. Reduced Graphene Oxide/copper Nanowire Hybrid Films as High-Performance Transparent Electrodes. *ACS Nano* **2013**, *7* (2), 1811–1816.

(25)   Zilberberg, K.; Gasse, F.; Pagui, R.; Polywka, A.; Behrendt, A.; Trost, S.; Heiderhoff, R.; Görrn, P.; Riedl, T. Highly Robust Indium-Free Transparent Conductive Electrodes Based on Composites of Silver Nanowires and Conductive Metal Oxides. *Adv. Funct. Mater.* **2014**, *24* (12), 1671–1678.

(26)   Chang, Y.-M.; Yeh, W.-Y.; Chen, P.-C. Highly Foldable Transparent Conductive Films Composed of Silver Nanowire Junctions Prepared by Chemical Metal Reduction. *Nanotechnology* **2014**, *25* (28), 285601.

(27)   Ahn, Y.; Jeong, Y.; Lee, Y. Improved Thermal Oxidation Stability of Solution-Processable Silver Nanowire Transparent Electrode by Reduced Graphene Oxide. *ACS Appl. Mater. Interfaces* **2012**, *4* (12), 6410–6414.

(28)   Ahn, Y.; Jeong, Y.; Lee, D.; Lee, Y. Copper Nanowire–Graphene Core–Shell Nanostructure for Highly Stable Transparent Conducting Electrodes. *ACS Nano* **2015**, *9* (3), 3125–3133.

(29)   Zhu, S.; Gao, Y.; Hu, B.; Li, J.; Su, J.; Fan, Z.; Zhou, J. Transferable Self-Welding Silver Nanowire Network as High Performance Transparent Flexible Electrode. *Nanotechnology* **2013**, *24* (33), 335202.

(30)   Madaria, A. R.; Kumar, A.; Ishikawa, F. N.; Zhou, C. Uniform, Highly Conductive, and Patterned Transparent Films of a Percolating Silver Nanowire Network on Rigid and Flexible Substrates Using a Dry Transfer Technique. *Nano Res.* **2010**, *3* (8), 564–573.

(31) Kubaschewski, O.; Hopkins, B. E. *Oxidation of Metals and Alloys*, 2nd ed.; Butterworths Scientific Publications, London, 1962.

(32) Hodges, R. J.; Pickering, W. F. The Oxidation of Hydrazine by silver(I) Oxide. *Aust. J. Chem.* **1966**, *19* (6), 981–991.

(33) Park, S.; Hu, Y.; Hwang, J. O.; Lee, E.-S.; Casabianca, L. B.; Cai, W.; Potts, J. R.; Ha, H.-W.; Chen, S.; Oh, J.; Kim, S. O.; Kim, Y.-H.; Ishii, Y.; Ruoff, R. S. Chemical Structures of Hydrazine-Treated Graphene Oxide and Generation of Aromatic Nitrogen Doping. *Nat. Commun.* **2012**, *3*, 638.

(34) Nickel, U.; zu Castell, A.; Pöppl, K.; Schneider, S. A Silver Colloid Produced by Reduction with Hydrazine as Support for Highly Sensitive Surface-Enhanced Raman Spectroscopy †. *Langmuir* **2000**, *16* (23), 9087–9091.

(35) Lee, J.; Lee, I.; Kim, T.-S.; Lee, J.-Y. Efficient Welding of Silver Nanowire Networks without Post-Processing. *Small* **2013**, *9* (17), 2887–2894.

(36) De, S.; Higgins, T. M.; Lyons, P. E.; Doherty, E. M.; Nirmalraj, P. N.; Blau, W. J.; Boland, J. J.; Coleman, J. N. Silver Nanowire Networks as Flexible, Transparent, Conducting Films Extremely High DC to Optical Conductivity Ratios. *ACS Nano* **2009**, *3* (7), 1767–1774.

(37) Moon, I. K.; Kim, J. Il; Lee, H.; Hur, K.; Kim, W. C.; Lee, H. 2D Graphene Oxide Nanosheets as an Adhesive Over-Coating Layer for Flexible Transparent Conductive Electrodes. *Sci. Rep.* **2013**, *3*, 1112.

(38) Schriver, M.; Regan, W.; Gannett, W. J.; Zaniewski, A. M.; Crommie, M. F.; Zettl, A. Graphene as a Long-Term Metal Oxidation Barrier: Worse than Nothing. *ACS Nano* **2013**, *7* (7), 5763–5768.

(39) Krantz, J.; Stubhan, T.; Richter, M.; Spallek, S.; Litzov, I.; Matt, G. J.; Spiecker, E.; Brabec, C. J. Spray-Coated Silver Nanowires as Top Electrode Layer in Semitransparent P3HT:PCBM-Based Organic Solar Cell Devices. *Adv. Funct. Mater.* **2013**, *23* (13), 1711–1717.

(40) Guo, F.; Kubis, P.; Stubhan, T.; Li, N.; Baran, D.; Przybilla, T.; Spiecker, E.; Forberich, K.; Brabec, C. J. Fully Solution-Processing Route toward Highly Transparent Polymer Solar Cells. *ACS Appl. Mater. Interfaces* **2014**, *6* (20), 18251–18257.

(41) Chen, C.-C.; Dou, L.; Zhu, R.; Chung, C.-H.; Song, T.-B.; Zheng, Y. B.; Hawks, S.; Li, G.; Weiss, P. S.; Yang, Y. Visibly Transparent Polymer Solar Cells Produced by Solution Processing. *ACS Nano* **2012**, *6* (8), 7185–7190.

(42) Wang, D. H.; Kyaw, A. K. K.; Gupta, V.; Bazan, G. C.; Heeger, A. J. Enhanced Efficiency Parameters of Solution-Processable Small-Molecule Solar Cells Depending on ITO Sheet Resistance. *Adv. Energy Mater.* **2013**, *3* (9), 1161–1165.

(43) Noh, Y.-J.; Kim, S.-S.; Kim, T.-W.; Na, S.-I. Effect of Sheet Resistance of Ag-Nanowire-Based Electrodes on Cell-Performances of ITO-Free Organic Solar Cells. *Semicond. Sci. Technol.* **2013**, *28* (12), 125008.

(44) Selzer, F.; Weiß, N.; Kneppe, D.; Bormann, L.; Sachse, C.; Gaponik, N.; Eychmüller, A.; Leo, K.; Müller-Meskamp, L. A Spray-Coating Process for Highly Conductive Silver Nanowire Networks as the Transparent Top-Electrode for Small Molecule Organic Photovoltaics. *Nanoscale* **2015**, *7* (6), 2777–2783.

(45) Yang, C.; Gu, H.; Lin, W.; Yuen, M. M.; Wong, C. P.; Xiong, M.; Gao, B. Silver Nanowires: From Scalable Synthesis to Recyclable Foldable Electronics. *Adv. Mater.* **2011**, *23* (27), 3052–3056.

(46) Ye, S.; Rathmell, A. R.; Stewart, I. E.; Ha, Y.-C.; Wilson, A. R.; Chen, Z.; Wiley, B. J. A Rapid Synthesis of High Aspect Ratio Copper Nanowires for High-Performance Transparent Conducting Films. *Chem. Commun.* **2014**, *50* (20), 2562–2564.

(47) Baek, S.-W.; Noh, J.; Lee, C.-H.; Kim, B.; Seo, M.-K.; Lee, J.-Y. Plasmonic Forward Scattering Effect in Organic Solar Cells: A Powerful Optical Engineering Method. *Sci. Rep.* **2013**, *3*, 1726.

(48) Yu, L.; Lim, Y.-S.; Han, J. H.; Kim, K.; Kim, J. Y.; Choi, S.-Y.; Shin, K. A Graphene Oxide Oxygen Barrier Film Deposited via a Self-Assembly Coating Method. *Synth. Met.* **2012**, *162* (7-8), 710–714.

(49) Born, P.; Blum, S.; Munoz, A.; Kraus, T. Role of the Meniscus Shape in Large-Area Convective Particle Assembly. *Langmuir* **2011**, *27* (14), 8621–8633.

(50) Baek, S.-W.; Park, G.; Noh, J.; Cho, C.; Lee, C.-H.; Seo, M.-K.; Song, H.; Lee, J.-Y. Au@Ag Core–Shell Nanocubes for Efficient Plasmonic Light Scattering Effect in Low Bandgap Organic Solar Cells. *ACS Nano* **2014**, *8* (4), 3302–3312.

(51) Jeong, S.; Cho, C.; Kang, H.; Kim, K.-H.; Yuk, Y.; Park, J. Y.; Kim, B. J.; Lee, J.-Y. Nanoimprinting-Induced Nanomorphological Transition in Polymer Solar Cells: Enhanced Electrical and Optical Performance. *ACS Nano* **2015**, *9* (3), 2773–2782.
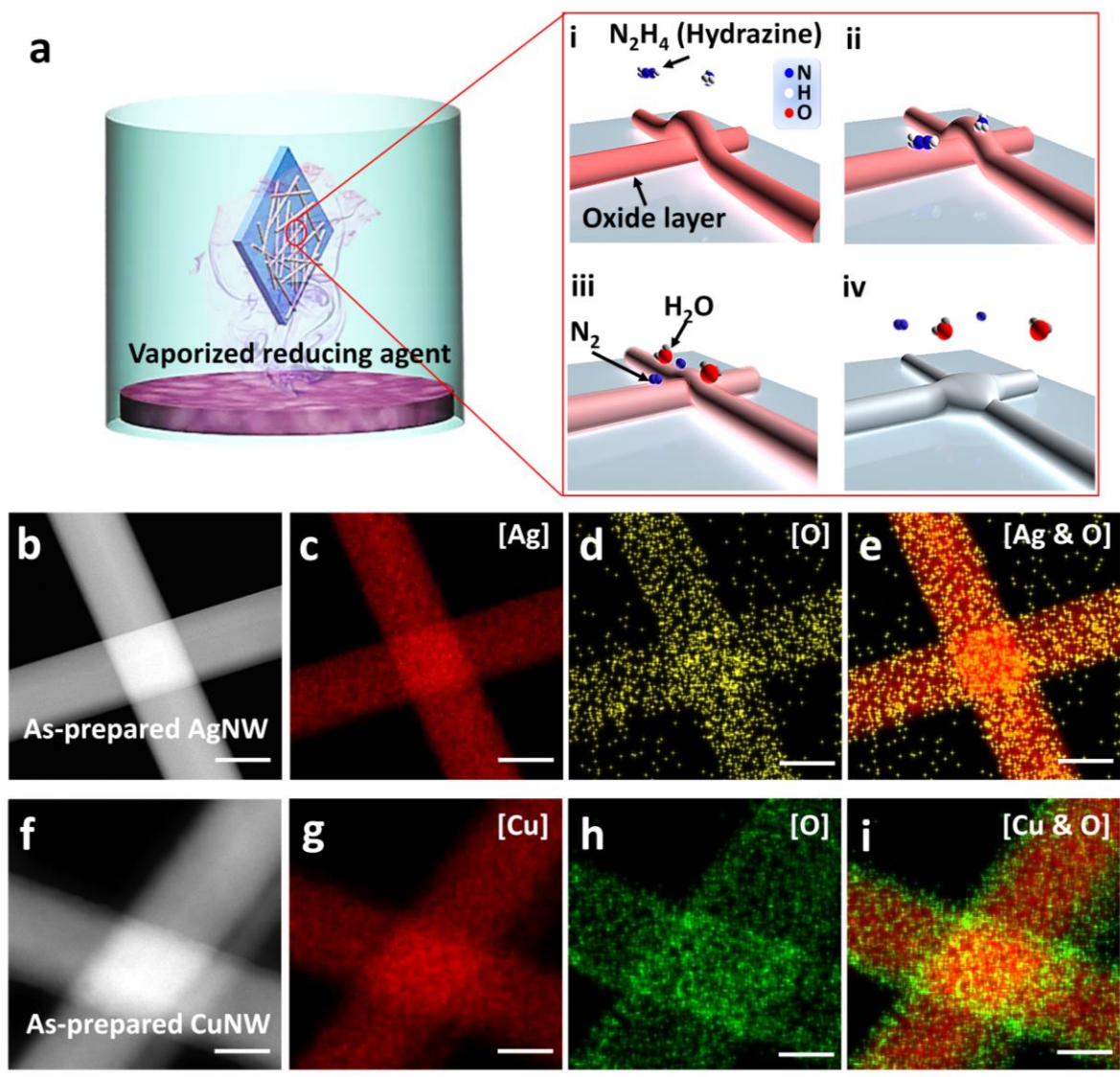
Figure 1. (a) Schematic illustration of oxide reduction of metal nanostructure by vaporized hydrazine. Red surfaces present the oxidized AgNWs in air. TEM and EDS mapping images of as-prepared (b-e) AgNWs and (f-i) CuNWs. Even fresh AgNWs and CuNWs have oxide layer on the surface. Scale bar: 80 nm
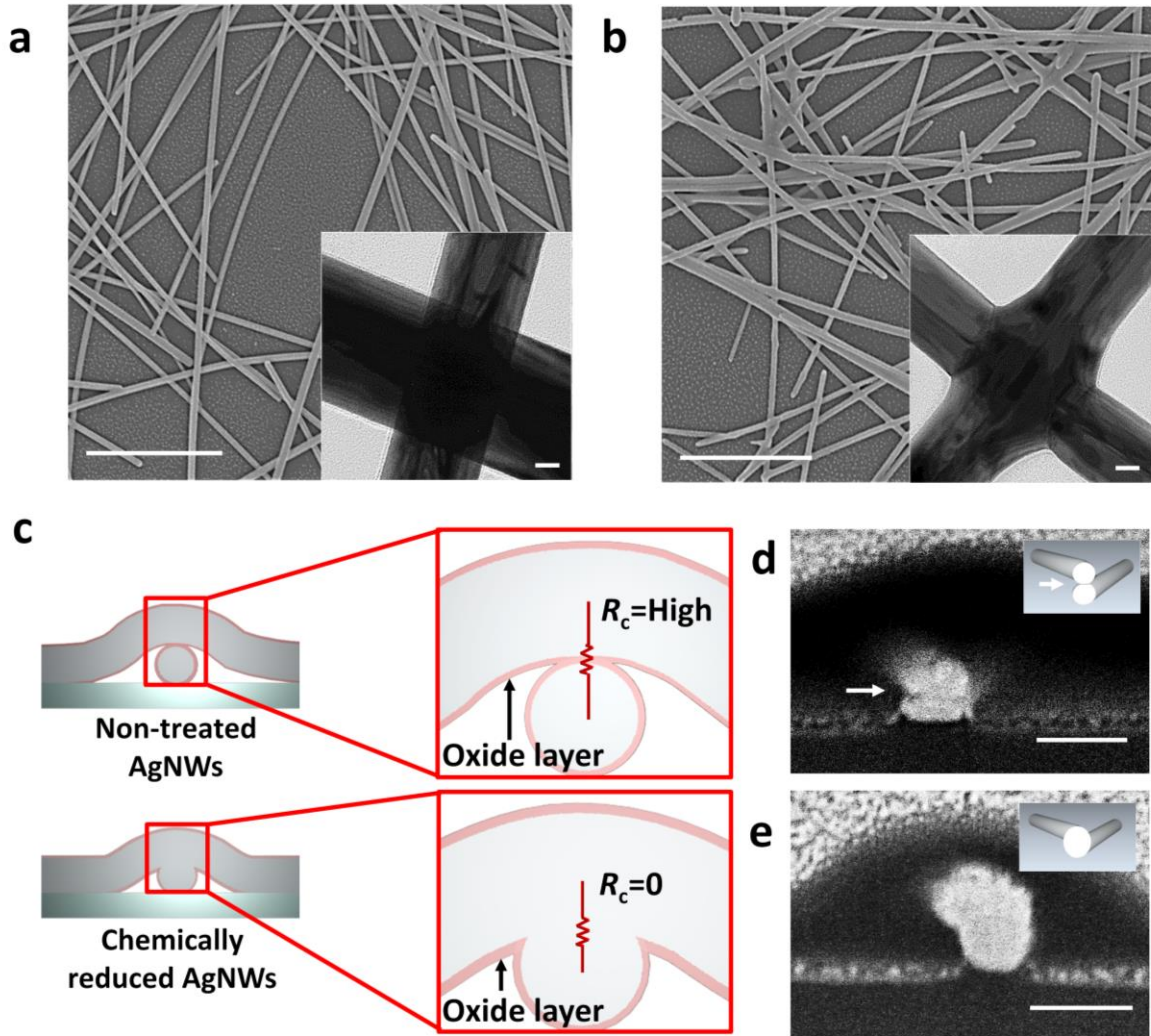
Figure 2. Top view of SEM images (a) before and (b) after reduction of the AgNWs. The inset images of (a) and (b) show TEM images that reveal the fused AgNWs after the reducing process. The scale bars in (a,b), and inset images represent 1 μm and 20 nm, respectively. (c) Schematic view of non-treated and reduced AgNW junctions. Contrary to non-treated AgNWs, reduced AgNWs are fully connected without subsequent oxidation. R_c denotes the contact resistance. Cross-sectional SEM images of AgNW junctions (d) before and (e) after reduction. (AgNW junction boundary is indicated by a white arrow) Scale bar: 100 nm. Inset images: schematic illustration of cross-sectional images.
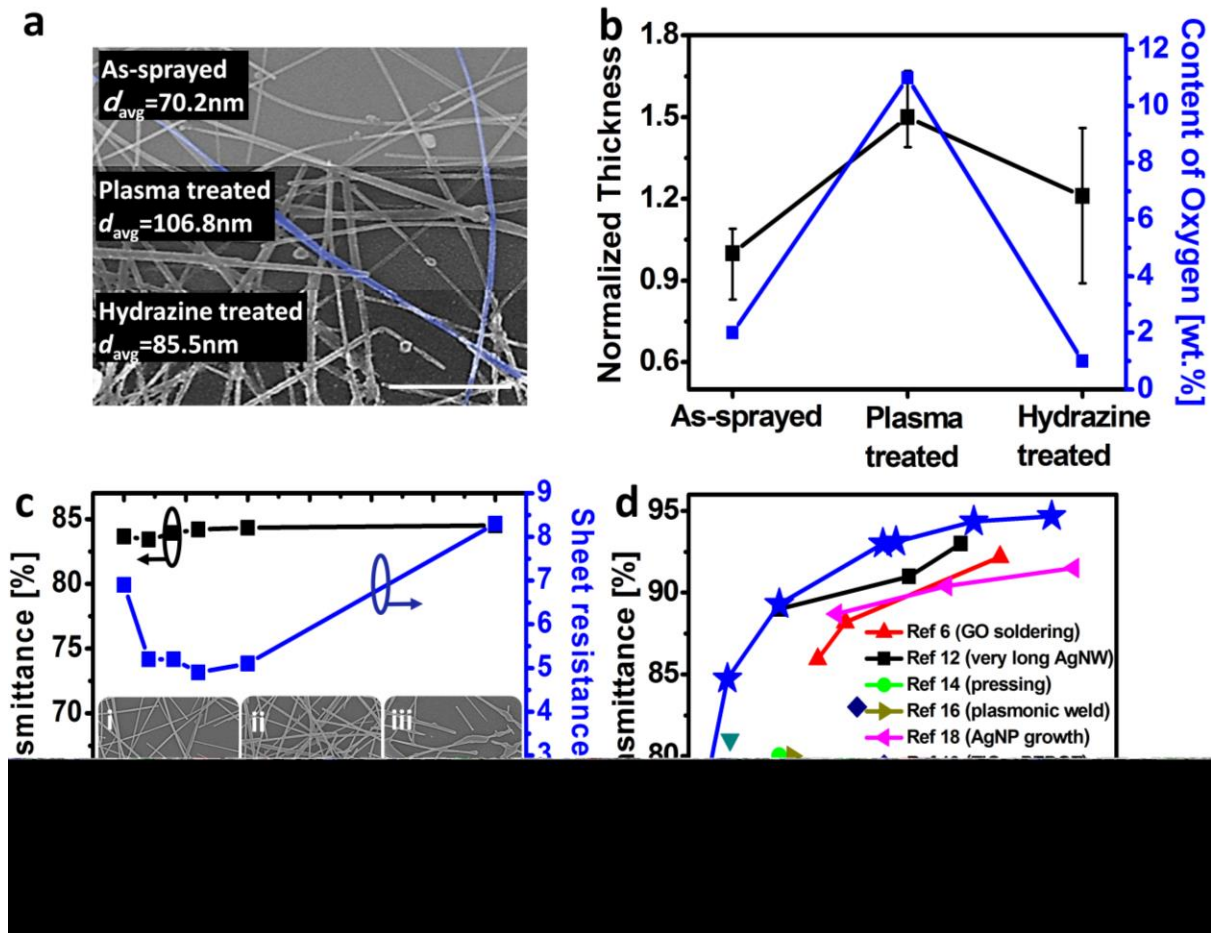
Figure 3. (a) SEM images of as-sprayed, plasma treated, and hydrazine treated AgNW networks taken at the same position. AgNWs become thick after plasma treatment and thin again by the subsequent hydrazine treatment. The average thickness d_{avg} values and blue colored AgNWs present the varied thickness after each treatment. Scale bar: 2 μm. (b) Normalized thickness of AgNWs and oxygen content acquired from EDS data in pristine state (left), after plasma (middle), and subsequent hydrazine treatments (right). (c) Transmittance (left scale) and sheet resistance (right scale) according to the hydrazine reduction time. The inset images (i–iii) are the SEM micrographs of AgNWs reduced for 0, 7, and 60 min, respectively. Scale bar: 1 μm. (d) Comparison of optoelectrical performance of AgNWs treated by hydrazine with previous reports.

23
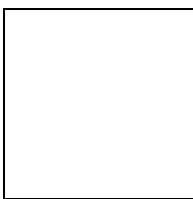
Figure 4. (a) Resistance changes of non-treated, GO coated, thermally annealed, and hydrazine treated AgNWs over exposure time in air. (b) Resistance changes of stretched AgNWs.
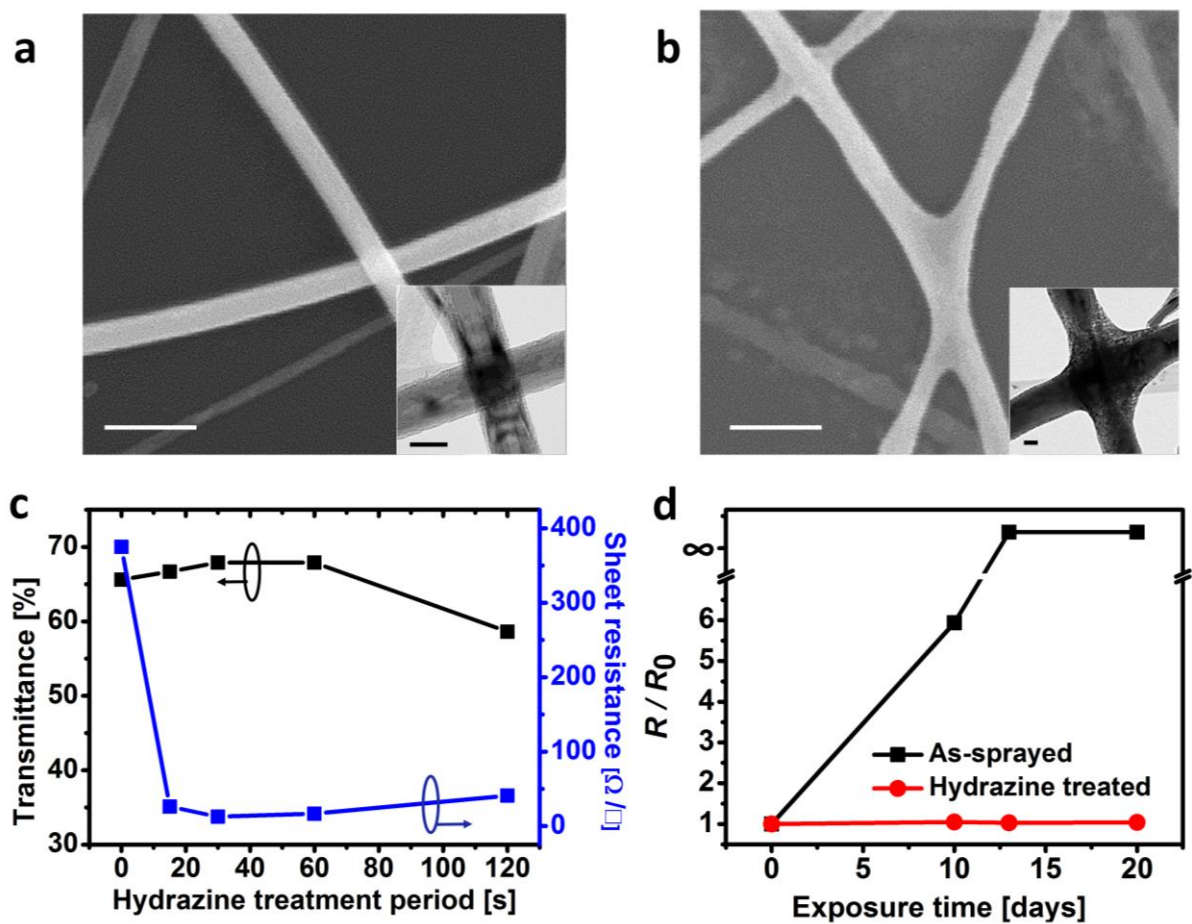
Figure 5. Top view of SEM and TEM images (inset) of CuNWs (a) before and (b) after

reduction treatment. After reduction treatment, CuNWs junctions are fused. Scale bar: 200 nm

(Inset scale bar: 40 nm) (c) Transmittance (left) and sheet resistance (right) of CuNWs

according to the hydrazine reduction time. (d) Resistance change of non-treated and hydrazine

treated CuNWs over exposure time in air.
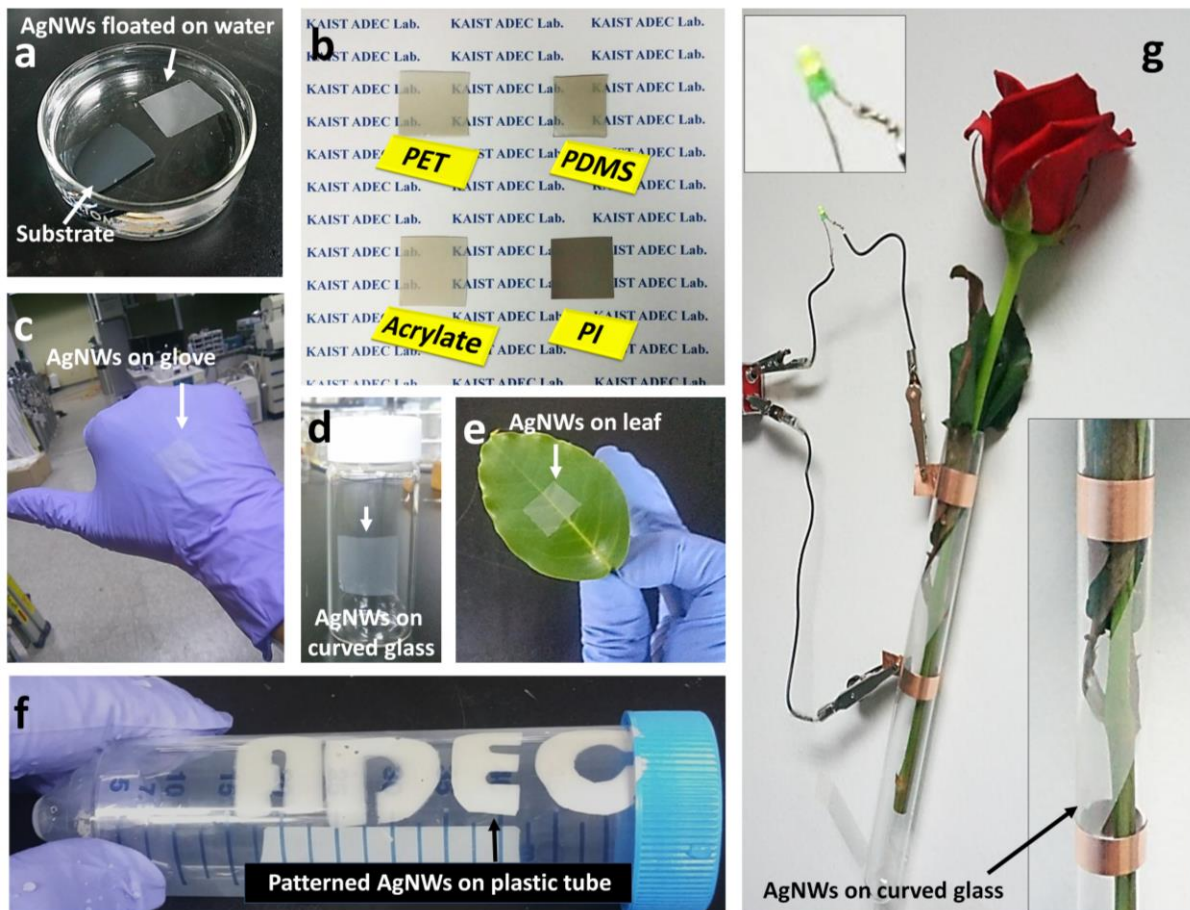
Figure 6. (a) AgNW network detached from the substrate and floating on the water. (b–f) Transferred AgNWs on (b) PET, PDMS, polyacrylate and polyimide, (c) a latex glove, (d) a curved glass, (e) a leaf, and (f) patterned AgNWs forming letters on the centrifuge tube. (g) Transferred AgNWs on curved glass lighting the LED.
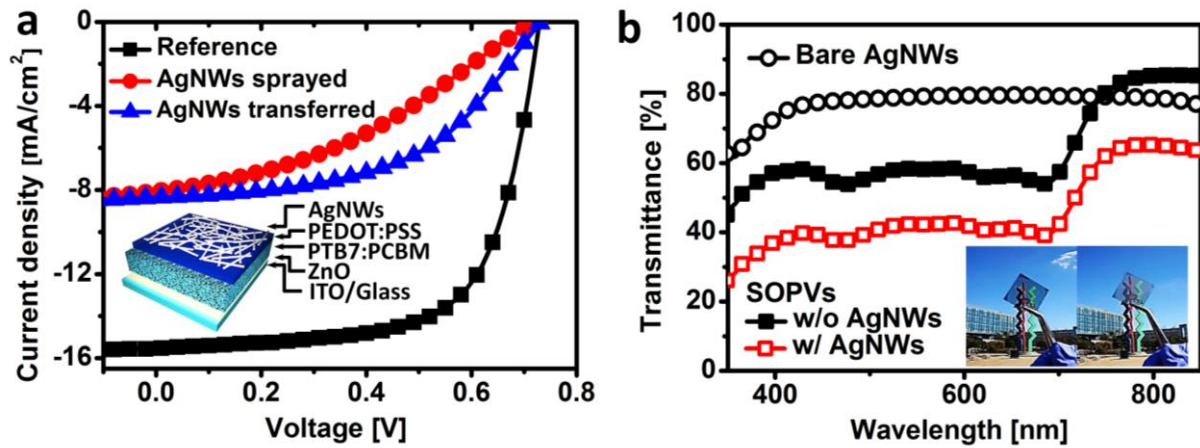
Figure 7. (a) Current density–voltage (*J*–*V*) characteristics of the SOPVs. Inset: schematic set-up of the SOPVs using AgNWs as top electrode. (b) Transmittance of bare AgNWs and SOPVs with and without AgNW electrode. Insets are photographs of the SOPVs with and without AgNW electrode in front of Carillon in KAIST.

Tables

Table 1. Performance of inverted PTB7:PC$_{70}$BM semi-transparent OPVs

Inverted PTB7:PC$_{70}$BM OPVs	J_{sc} [mA/cm^2]	V_{oc} [V]	*FF*	PCE [%]
Reference	15.52	0.73	0.67	7.54
AgNWs sprayed	8.08	0.72	0.36	2.12
AgNWs transferred	8.36	0.73	0.51	3.11

Table of Contents Graphic
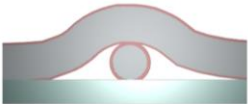
Non-treated AgNWs

Chemically reduced AgNWs

AgNWs transferred on leaf